remote sensing

MDPI

Article

Evaluating an Enhanced Vegetation Condition Index (VCI) Based on VIUPD for Drought Monitoring in the Continental United States

Wenzhe Jiao [1,2], Lifu Zhang [1,*], Qing Chang [2,3], Dongjie Fu [1], Yi Cen [1] and Qingxi Tong [1]

1 State Key Laboratory of Remote Sensing Science, Institute of Remote Sensing and Digital Earth, Chinese Academic of Science, Beijing 100101, China; jiaowz@radi.ac.cn (W.Z.); fudj@raid.ac.cn (D.F.); cenyi@radi.ac.cn (Y.C.); tongqx@radi.ac.cn (Q.T.)
2 University of Chinese Academy of Science, Beijing No. 19A Yuquan Road, Beijing 100049, China; hellochangqing@126.com
3 Key Laboratory of Digital Earth Science, Institute of Remote Sensing and Digital Earth, Chinese Academy of Sciences, Beijing 100094, China
* Correspondence: zhanglf@radi.ac.cn; Tel.: +86-10-6483-9450

Academic Editors: Xuepeng Zhao, Wenze Yang, Viju John, Hui Lu, Ken Knapp, Magaly Koch and Prasad S. Thenkabail
Received: 21 December 2015; Accepted: 4 March 2016; Published: 10 March 2016

Abstract: Drought is a complex hazard, and it has an impact on agricultural, ecological, and socio-economic systems. The vegetation condition index (VCI), which is derived from remote-sensing data, has been widely used for drought monitoring. However, VCI based on the normalized difference vegetation index (NDVI) does not perform well in certain circumstances. In this study, we examined the utility of the vegetation index based on the universal pattern decomposition method (VIUPD) based VCI for drought monitoring in various climate divisions across the continental United States (CONUS). We compared the VIUPD-derived VCI with the NDVI-derived VCI in various climate divisions and during different sub-periods of the growing season. It was also compared with other remote-sensing-based drought indices, such as the temperature condition index (TCI), precipitation condition index (PCI) and the soil moisture condition index (SMCI). The VIUPD-derived VCI had stronger correlations with long-term *in situ* drought indices, such as the Palmer Drought Severity Index (PDSI) and the standardized precipitation index (SPI-3, SPI-6, SPI-9, and SPI-12) than did the NDVI-derived VCI, and other indices, such as TCI, PCI and SMCI. The VIUPD has considerable potential for drought monitoring. As VIUPD can make use of the information from all the observation bands, the VIUPD-derived VCI can be regarded as an enhanced VCI.

Keywords: drought monitoring; VCI; VIUPD; NDVI; MODIS

---

1. Introduction

Drought is the most costly disaster that can affect natural habitats, ecosystems, agricultural systems, and urban water supplies [1,2]. As a result, many techniques for monitoring drought conditions have been developed.

The complex drought phenomenon can be simplified into a drought index, which is a single number incorporating a large amount of water supply and water demand data [3]. A variety of drought indices have been developed [1]. Many were derived using station-based measurements of temperature and precipitation, such as the Palmer drought severity index (PDSI), the moisture anomaly index (Z-index) [4], and the standardized precipitation index (SPI) [5]. These drought indices can effectively evaluate drought conditions around meteorological stations, but the lack of continuous spatial coverage limits the ability to characterize and monitor the detailed spatial pattern of drought conditions on a regional scale, especially in areas with few meteorological stations or a high degree of spatial variability [2].

Remote-sensing technology has made it possible to monitor soil moisture and the condition of vegetation across large areas. In locations with a limited number of sampling gauges, remote sensing data may be the only available information source for drought monitoring [6,7]. Satellite-based drought indices such as the normalized difference vegetation index (NDVI)-based vegetation condition index (VCI) [8] have been widely used for detecting the onset of drought and measuring the intensity, duration, and impact of drought globally [8–15]. The obvious advantage of VCI is that it can be easily computed owing to the fact that it does not require station observation data, and as a satellite-based drought product it can provide near real-time data over the globe at a relatively high spatial resolution [16].

The utility of the NDVI-derived VCI for monitoring drought conditions has been studied in various regions around the world and has been shown to be strongly correlated with agricultural production in regions of South America, Africa, Asia, North America, and Europe, particularly during the critical periods of crop growth [17]. The VCI based on NDVI has also been compared with vegetation density, biomass, and field reflectance measurements in Kazakhstan and has proven to be a good indicator of the impact of weather on vegetation conditions and health [18]. However, other studies have shown that the NDVI-derived VCI should be used with caution. When the NDVI-derived VCI and other satellite-derived drought indices were compared to station-based drought indices over the desert and desert steppe regions of Mongolia, they showed little agreement [19]. A similar situation was observed in India, where the NDVI-derived VCI alone was shown to be insufficient for drought monitoring [14]. The NDVI-derived VCI was also tested in different counties in Texas, U.S.; the correlations between the NDVI-derived VCI and *in situ* drought indices varied greatly among counties [20].

The aim of most studies has been to establish drought indices with simple input data, and only a simple calculation [21]. Kogan *et al.* [17] established VCI and temperature condition index (TCI) with a simple and efficient formula. Later, the widely used precipitation condition index (PCI) and soil moisture condition index (SMCI) which were derived from the Tropical Rainfall Measuring Mission (TRMM) data and ARMS-E data respectively, were also established based on the same formula [2]. For vegetation index, most of the studies focused on the VCI derived from NDVI, whereas few studies have considered drought monitoring using other easily calculated vegetation indices. The vegetation index based on the universal pattern decomposition method (VIUPD), which was established by Zhang *et al.* [22], has several advantages over other vegetation indices. Like NDVI, VIUPD is also based on satellite-based data and can provide near real-time data over the globe at a relatively high spatial resolution. This index reflects biophysical factors, such as vegetation concentrations and the degree of terrestrial vegetation vigor. Unlike the traditional broadband vegetation indices that are usually computed using the near-infrared and red bands, VIUPD is based on all observed bands. Narrowband hyperspectral data-based VIUPD has been proven to be sensitive to spectral operations and was more sensor-independent than the other 11 vegetation indices, including the NDVI and EVI [23]. VIUPD also showed great potential to discern variations in urban LST when it was used to analyze the urban heat island effect in Shijiazhuang, China [24]. VIUPD was also applied to the inversion of crop chlorophyll content, and was found to have greater accuracy and stability when estimating the chlorophyll content of winter wheat than the NDVI, the triangle vegetation index (TVI), and the ratio of modified transformed chlorophyll absorption ratio index [25]. However, the utility of VIUPD for drought monitoring in large and different climate regions remains unknown.

In this study, we established another type of VCI with VIUPD as a new drought monitoring index. The strength and weakness of VIUPD-derived VCI for drought monitoring in various climate divisions across the continental United States (CONUS) were evaluated by comparing the VIUPD-derived VCI and other remote-sensing-based drought indices to traditional station-based drought indices.

2. Materials and Methods

2.1. Study Area

In this study, the study area is located in the continental United States. The National Land Cover Database 2011 (NLCD2011) was used to illustrate the spatial distributions of different land covers. According to NLCD2011, the cropland and grassland make up most of the land cover in the Great Plains; deciduous forests mainly locate in the east while evergreen forests in the west; shrubs are distributed in west and south western regions and woody wet lands are close to Great Lakes and along the coastline in the east (Figure 1).

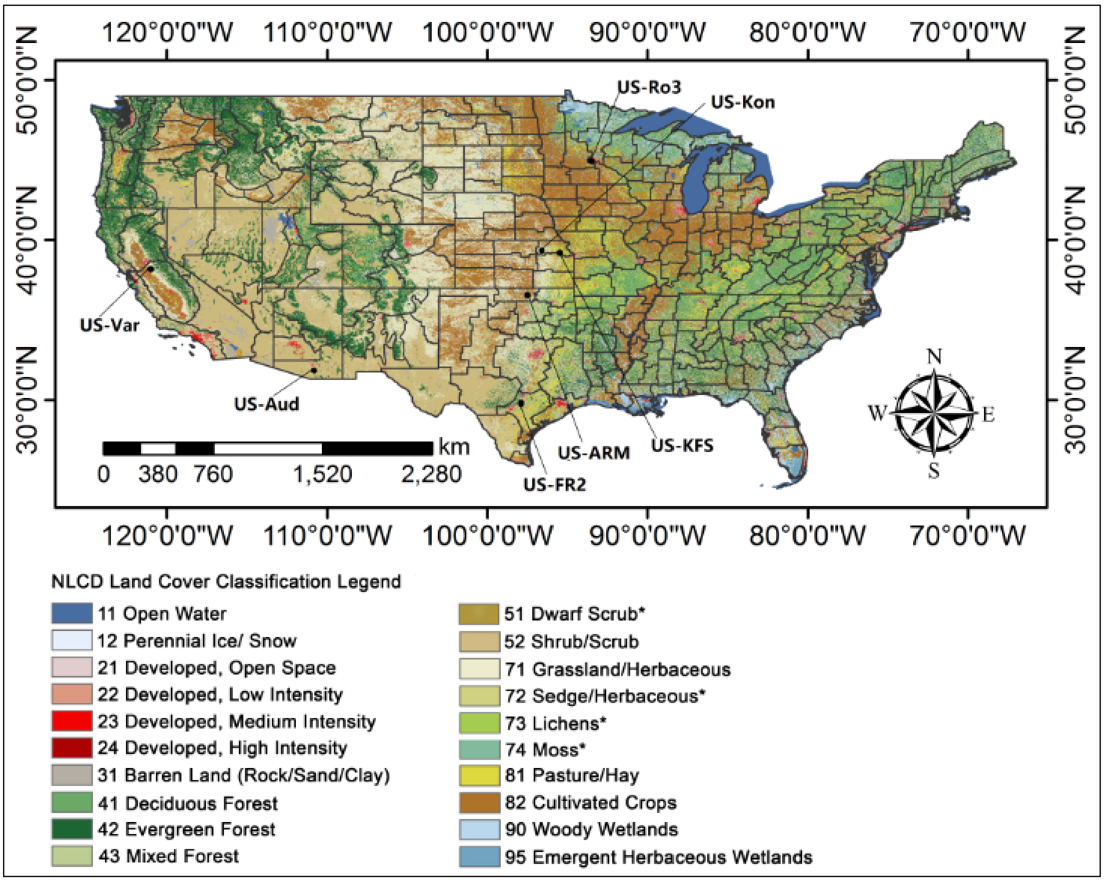

Figure 1. Location of the study area. The study area was divided into different climate divisions and the US-ARM, US-Aud, US-KFS, US-FR2, US-Kon, US-Ro3 and US-Var are names of the flux tower sites. The black circles are their geographic positions.

The basic geographic unit of this study is the climate division (CD), which is defined by the National Climate Data Center (NCDC). The continental United States (CONUS) is divided into 344 CDs. Each CD represents relatively homogenous climate characteristics such as temperature and precipitation. The distribution data and complete details about the climate divisions are available at NCDC [26].

2.2. Station-Based Drought Indices

The station-based drought indices of PDSI, moisture anomaly index (Z-index) and SPI were selected for evaluating the remote-sensing based drought indices. The National Climate Data Center (NCDC) has made monthly Z-index, PDSI, and SPI records available from 1895 to the present day [26]. These *in situ* indices have been used in various studies to evaluate remote-sensing drought indices [7,16,20,27,28]. The PDSI and Z-index are calculated using a soil moisture balance algorithm that requires not only a time series of daily air temperature and precipitation data, but also information on the available water content of the soil. The Z-index for the month i is calculated basing the formula below:

$$Z_i = d_i K_i, \tag{1}$$

where Z_i is the Z-index for month i, K_i is a weighting factor that is initially determined by an empirically derived coefficient $K\prime$ using the formula below:

$$K_i = \frac{14.2}{\sum D_i K_i} K\prime, \tag{2}$$

where D is obtained using the calibration period by determining the of the absolute values for each month of the year. The relationship between PDSI and Z-index is as below:

$$PDSI_i = \frac{Z_i}{3} + 0.897 PDSI_{i-1}, \tag{3}$$

where $PDSI_i$ is the PDSI for month i, Z_i is the Z-index for month i, $PDSI_{i-1}$ is the PDSI of the month $i-1$. Complete details on how to calculate PDSI and Z-index are available in Palmer *et al.* [4].

The SPI is calculated by standardizing the probability of observed precipitation for any duration of interest (e.g., weeks, months, or years). Durations of weeks or months can be used to apply the SPI for agricultural or meteorological purposes, and longer durations of years can be used to apply it for hydrological and water management purposes [4,29]. In this study, the monthly precipitation data was used and the 1-, 3-, 6-, 9-, 12-, and 24-month SPI were calculated for each climate division region (specified as SPI-1, SPI-3, SPI-6, SPI-9, SPI-12 and SPI-24, respectively, in this study).

2.3. Flux Tower GPP Data

The monthly gap-filled flux estimated gross primary production (GPP) was selected as the drought impact data to evaluate the VIUPD-derived VCI in this study. The *in situ* data on GPP were measured by an eddy covariance instrument set on the flux tower. The GPP data can be downloaded from the AmeriFlux website [30]. The months from April to October are chosen. As the VIUPD is a vegetation index and VIUPD-derived VCI is mainly suitable for monitoring agricultural drought, we chose the grass and crop vegetation types covering comparatively longer period sites in this study. Table 1 shows the details of the chosen flux sites and Figure 1 shows their geographic positions.

Table 1. Flux sites used in this study.

Site Name	Loc_Lat	Loc_Long	Elevation	Vegetation Type	Active or Not
US-ARM	36.6058	−97.4888	314	crop	Active
US-Aud	31.5907	−110.51	1469	grass	Active
US-FR2	29.9495	−97.9962	272	grass	Active
US-FR3	29.94	−97.99	232	grass	Active
US-KFS	39.0561	−95.1907	310	grass	Active
US-Kon	39.0824	−96.5603	330	grass	Active
US-Ro3	44.7217	−93.0893	260	crop	Active
US-Var	38.4133	−120.951	129	grass	Active

2.4. Remote Sensing Data

The moderate-resolution imaging spectroradiometer (MODIS) covers the entire surface of the Earth every 1–2 days, and other biophysical quantities, at resolutions between 250 m and 1 km. In this work, the NDVI was calculated based on MOD09A1 data obtained from the Land Processes Distributed Active Center (LPDAAC) [31]. Eight-day LST data with a 1-km resolution (MOD11A2) were obtained from the National Aeronautics and Space Administration's (NASA) earth observing system data and information system (EOSDIS) [32]. Seventeen tiles of MODIS data (h07v06, h08-h13, v04-v06) were used to cover the CONUS, and data from 89 to 297 days of each year were used to cover the primary growing season of most vegetation types. Eight-day images were composited into monthly data, weighted by the number of days recorded in each month, and based on the data generated after masking the cloud value pixels, using MODIS data quality flags.

The Tropical Rainfall Measuring Mission (TRMM) 3B43 data, which were obtained from the NASA Data and Information Services Center (DISC) and the Advanced Microwave Scanning Radiometer-Earth Observing System (AMSR-E), which were obtained from the Vrije Universtiteit Amsterdam [33] and NASA (VUA-NASA), were also used in this study.

2.5. Vegetation Condition Index

The NDVI is widely used to estimate the density and health of vegetation. Because of the close relationship between vegetation vigor and available soil moisture, it has been used to monitor drought conditions. The maximum value composites (MVC) method was used to composite the eight-day images to monthly data. The VIUPD is computed based on the universal pattern decomposition approach [22]. It can be computed as a combination of four pattern decomposition coefficients: the patterns of vegetation, soil, and water, and the supplementary pattern.

$$VIUPD = \frac{C_V - a \times C_S - C_4}{C_W + C_V + C_S}, \tag{4}$$

where C_V, C_S, C_W and C_4 represent the standard pattern reflectance of vegetation, soil, water, and the supplementary pattern, respectively. a is a empirical coefficient and defined as 0.1 according to the experiments conducted by Zhang *et al.* [22]. In this study, eight-day MODIS surface reflectance data (MOD09A1) were used to calculate VIUPD based on the formula above. The C_V, C_S, C_W and C_4 are determined by the formula below:

$$R_i = C_w P_{iw} + C_v P_{iv} + C_s P_{is} + C_4 P_{i4}, \tag{5}$$

where, R_i is the reflectance of band i measured by MOD09A1, C_V, C_S, C_4 and C_W are the decomposition coefficients for vegetation, soil, supplement and water respectively, and P_{iw}, P_{iv}, and P_{is} are the respective standard spectral patterns for water, vegetation and soil for MODIS sensor. P_{i4} is the supplementary standard pattern for i bands and a yellow-leaf spectrum is used in this study. Formula (5) can also be expressed using matrix notations as follow:

$$R = PC + r, \tag{6}$$

where $R = (R_1, R_2, \ldots, R_n)^{\mathrm{T}}$ is the vector of reflectance, n is the number of spectral bands which in this study is 7. $P = (P_w, P_v, P_s, P_4)$ is the 7×4 matrix for band number 7, C = $(C_w, C_v, C_s, C_4)^{\mathrm{T}}$ is the column vector of coefficients and r is the residual column vector for band i. By minimizing the sum-of-squared-error criterion function yields of Equation (6), we can get the values of C_w, C_v, C_s and C_4.

Eight-day images of VIUPD were composited into monthly data, weighted by the number of days recorded in each month, and based on the data generated after masking the cloud value pixels, using MODIS data quality flags.

The VCI was developed to control for local differences in ecosystem productivity. The VCI is a pixel-wise normalization of VI that is useful for making relative assessments (e.g., pixel-specific) of changes in the VI signal by filtering out the contribution of local geographic resources to the spatial variability of VI. The *VCI* is computed as:

$$VCI_{ijk} = \frac{VI_{ijk} - VI_{i,\min}}{VI_{i,\max} - VI_{i,\min}}, \tag{7}$$

where V_{ijk} represents the monthly VI for pixel i in month j for year k, and $V_{i,max}$ and $V_{i,min}$ denote the multiyear minimum and maximum VI, respectively, for pixel i in month j. In this study, NDVI-derived VCI and VIUPD-derived VCI were computed based on the formula above wherein VI is replaced by NDVI and VIUPD, respectively. The VCI values were averaged spatially to climate division level to facilitate comparison with observation-based drought indices.

2.6. Other Data

A number of additional datasets were used in this study to evaluate the utility of the VIUPD-derived VCI for drought monitoring in the continental US. We used the United States drought monitor (USDM) as the reference data for evaluating the VIUPD-derived VCI. USDM combines information from multiple drought indicators, including PDSI, SPI, and local reports from state climatologists and observers throughout the country. USDM data [34] were classified into one of five categories: abnormally dry (D0), moderate drought (D1) (the first designated level of drought), severe drought conditions (D2), extreme drought (D3), and exceptional drought (D4).

Other remote sensing-based drought indices were also established to compare the performance of drought monitoring with the VIUPD-derived VCI. We also compared the VIUPD-derived VCI with other remote sensing-based drought indices, such as the temperature condition index (TCI), precipitation condition index (PCI), soil moisture condition index (SMCI). These remote sensing-based drought indices are described in Table 2.

Table 2. Description of the remote sensing-based drought indices.

Drought Index	Data Source	Method	Source
TCI	MODIS, AMSR-E	$(LST_{i,max} - LST_{ijk})/(LST_{i,max} - LST_{i,min})$	[17]
SMCI_VUA	AMSR-E	$(SM_{ijk} - SM_{i,min})/(SM_{i,max} - SM_{i,min})$	[2]
SMCI_NSIDC	AMSR-E	$(SM_{ijk} - SM_{i,min})/(SM_{i,max} - SM_{i,min})$	[2]
PCI	TRMM	$(TRM_{ijk} - TRM_{i,min})/(TRM_{i,max} + TRM_{i,min})$	[2]

LST_{ijk}, SM_{ijk}, $TRMM_{ijk}$—monthly LST, SM, TRMM for pixel i, in month j, for year k, respectively. $LST_{i,min}$, $SM_{i,min}$, $TRMM_{i,min}$—multi-year minimum LST, SM, TRMM, respectively, for pixel i. $LST_{i,max}$, $SM_{i,max}$, $TRMM_{i,max}$—multi-year maximum LST, SM, TRMM, respectively.

2.7. Validation of the VIUPD-Derived VCI

We evaluated the VIUPD-derived VCI in three stages. During the first stage, we selected the growing season (April–October) in 2011 as the drought year with which to evaluate the indices. The US, and Texas in particular, experienced a harsh drought in the summer of 2011 [19]. The drought conditions monitored from VIUPD-derived VCI were compared to the drought conditions monitored from NDVI-derived VCI and USDM. USDM was used as a standard for the comparison. The widespread use of the USDM makes this choice feasible; additionally, USDM has a certain level of subjectivity due to individuals' reports. In this stage, we used the visual comparison method; the VIUPD-derived VCI are closer to USDM than NDVI-derived VCI in spatial distribution.

In the second stage, we used the *in situ* drought indices as the standard data, and evaluated the performance of the VIUPD-derived VCI and NDVI-derived VCI using three goodness-of-fit measures: the correlation values (r-value), the root mean square error (RMSE), and the mean absolute error (MAE). In the comparison between the VIUPD-derived VCI and NDVI-derived VCI, the correlation values were calculated between VIUPD-derived VCI, NDVI-derived VCI, and SPI-1, SPI-3, SPI-6, SPI-9, SPI-12, SPI-24, Z-index, and PDSI in 334 climate divisions from May to October (in total, $2 \times 8 \times 7 \times 344 = 38528$ r-values). The total RMSE, MAE and 38528 r-values were used to evaluate the performance of VIUPD-derived VCI. The r-value, RMSE and MAE were calculated using the formulas below:

$$RMSE = \sqrt{N^{-1}\sum_{i=1}^{N}(X_i - Y_i)^2}, \quad (8)$$

$$MAE = N^{-1}\sum_{i=1}^{N} |X_i - Y_i|, \tag{9}$$

$$r = \frac{\sum_{i=1}^{N} (X_i - \overline{X})(Y_i - \overline{Y})}{\sqrt{\sum_{i=1}^{N} (X_i - \overline{X})^2}\sqrt{\sum_{i=1}^{N} (Y_i - \overline{Y})^2}}, \tag{10}$$

where X_i is the remote sensing-based drought index for point i; $\overline{X}$ is the mean value of the remote sensing-based drought indices; Y_i is the *in situ* drought index for point i; and $\overline{Y}$ is the mean value of the *in situ* drought indices.

In the third stage, we used the *in situ* drought indices as the standard data and compared the VIUPD-derived VCI with the commonly used remote sensing drought indices SMCI, TCI, PCI, and SMCI, derived from the Data and Information Services Center (NSIDC) and Vrije Universtiteit (VUA). We calculated the overall RMSE, MAE as well as the r-values in each of the 344 climate divisions from May to October.

3. Results

3.1. Monthly Temporal Correlations

The mean remote sensing-based drought index performance statistics for all 344 climate divisions are summarized in Tables 3–5. In this study, we compared the correlations between *in situ* drought indices (PDSI, Z-Index, 1-, 2-, 3-, 6-, 9-, 12-, and 24-month SPI) and seven remotely sensed drought indices (VIUPD-derived VCI, NDVI-derived VCI, TRMM-derived PCI, MODIS-derived TCI, VUA-derived TCI, VUA-derived SMCI and NSIDC-derived SMCI). Among the seven remotely sensed drought indices compared, VIUPD-derived VCI ranked first in most seven goodness-of-fit measures. As shown in Table 3, the VIUPD-derived VCI correlates best with PDSI, 3-, 6-, 9-, 12-, and 24-month SPI (r = 0.622, 0.564, 0.582, 0.584, 0.548, and 0.390 respectively), and Tables 4 and 5 indicated that it has less error with PDSI, 3-, 6-, 9-, 12-, and 24-month SPI (RMSE = 2.658, 1.075, 1.082, 1.058, 1.068, and 1.074, respectively, and MAE = 1.592, 0.892, 0.897, 0.873, 0.885, and 0.887, respectively) than those of NDVI-derived VCI, PCI, TCI and SMCI. However, in terms of correlations with the short-term drought indices (such as the Z-index and SPI-1), the performance of the VIUPD-derived VCI was worse than that of the PCI. The r-value for the VIUPD-derived VCI and SPI-1 was lower than that of the VUA-based SMCI (Table 3). This is mainly because the drought indices of PCI and VUA-based SMCI are meteorological indices. PCI is directly based on the precipitation data of TRMM and VUA-based SMCI is derived from soil moisture data from ARMS-E, while VIUPD is a vegetation index which measures the health condition of the vegetation. Previous studies revealed that there is a lag response of vegetation indices to moisture conditions and the lagged response of vegetation indices likely occurs because vegetation growth is controlled by soil moisture and therefore changes in vegetation growth are buffered by soil moisture [2,3]. 1- and 2-month SPI are more suitable for evaluating meteorological remote sensing-based drought indices such as PCI and VUA-based SMCI; PDSI, 3-, 6-, 9-, 12-, and 24-month SPI are more suitable for evaluating agricultural remote sensing-based drought indices [29,35].

Table 3. Comparisons of the r-value between VIUPD-derived VCI and other commonly used remote sensing-based single drought indices.

Drought Indices	r (n = 24,080)							
	PDSI	Z	SPI-1	SPI-3	SPI-6	SPI-9	SPI-12	SPI-24
VIUPD-VCI	0.622 *	0.313	0.234	0.564 *	0.582 *	0.584 *	0.548 *	0.390 *
NDVI-VCI	0.382	0.284	0.217	0.354	0.326	0.344	0.318	0.237
PCI	0.440	0.806	0.865 *	0.559	0.398	0.350	0.303	0.211
TCI	0.542	0.589	0.487	0.515	0.471	0.423	0.379	0.278
TCI-VUA	0.215	0.241	0.147	0.182	0.168	0.155	0.126	0.072
SMCI-VUA	0.370	0.451	0.426	0.389	0.331	0.297	0.259	0.197
SMCI-NSIDC	0.074	0.237	0.291	0.222	0.140	0.085	0.056	0.002

* denotes the maximum value in each column.

Table 4. Comparisons of RMSE between VIUPD-derived VCI and other commonly used remote sensing-based single drought indices.

Drought Indices	RMSE (n = 24,080)							
	PDSI	Z	SPI-1	SPI-3	SPI-6	SPI-9	SPI-12	SPI-24
VIUPD-VCI	2.658 *	2.244	1.159	1.075 *	1.082 *	1.058 *	1.068 *	1.074 *
NDVI-VCI	2.782	2.384	1.681	1.145	1.326	1.344	1.368	1.370
PCI	3.440	0.865	0.801 *	2.559	2.598	2.650	2.703	2.811
TCI	2.709	2.289	1.166	1.145	1.271	1.223	1.379	1.278
TCI-VUA	2.774	2.567	1.026	1.057	1.071	1.059	1.085	1.099
SMCI-VUA	2.856	2.234	1.183	1.324	1.245	1.255	1.265	1.278
SMCI-NSIDC	3.374	3.237	3.291	3.122	3.140	3.155	3.156	3.202

* denotes the minimum value in each column.

Table 5. Comparisons of MAE between VIUPD-derived VCI and other commonly used remote sensing-based single drought indices.

Drought Indices	MAE (n = 24,080)							
	PDSI	Z	SPI-1	SPI-3	SPI-6	SPI-9	SPI-12	SPI-24
VIUPD-VCI	1.592 *	1.819	0.871	0.892 *	0.897 *	0.873 *	0.885 *	0.887 *
NDVI-VCI	1.682	1.984	1.217	1.354	1.366	1.368	1.378	1.437
PCI	1.840	0.963	0.665*	0.959	1.198	1.350	1.403	1.511
TCI	1.642	1.967	0.987	0.915	0.971	0.923	0.979	0.978
TCI-VUA	2.198	1.767	0.867	0.885	0.897	0.879	0.901	0.910
SMCI-VUA	2.656	2.451	1.326	1.339	1.381	1.297	1.259	1.197
SMCI-NSIDC	3.074	3.267	2.991	2.222	0.240	2.285	2.356	2.402

* denotes the minimum value in each column.

3.2. Regional Drought Patterns Derived from NDVI and VIUPD-Derived VCI

The months of April to October 2011 were selected to exemplify the spatial variation of the indices for that in 2011, the U.S experienced one of the typical severe droughts in the history of the country. The drought map in Figure 2 shows a variation among the indices. In Figure 2, the VIUPD-derived VCI was compared against NDVI-derived VCI using only those months from April to October. This was done because these months represent the maximum vegetation growth and VCI is only useful for monitoring drought condition during the growing-season for it measures vegetation health. Another reason for choosing April to October is to exclude some noise effects in winter, such as snow. In Figure 2, the first column displays the observed USDM drought data for the period of April to October 2011, while the second, third and fourth columns show the NDVI-derived VCI, difference between the VIUPD-derived VCI and NDVI-derived VCI, and VIUPD-derived VCI respectively.

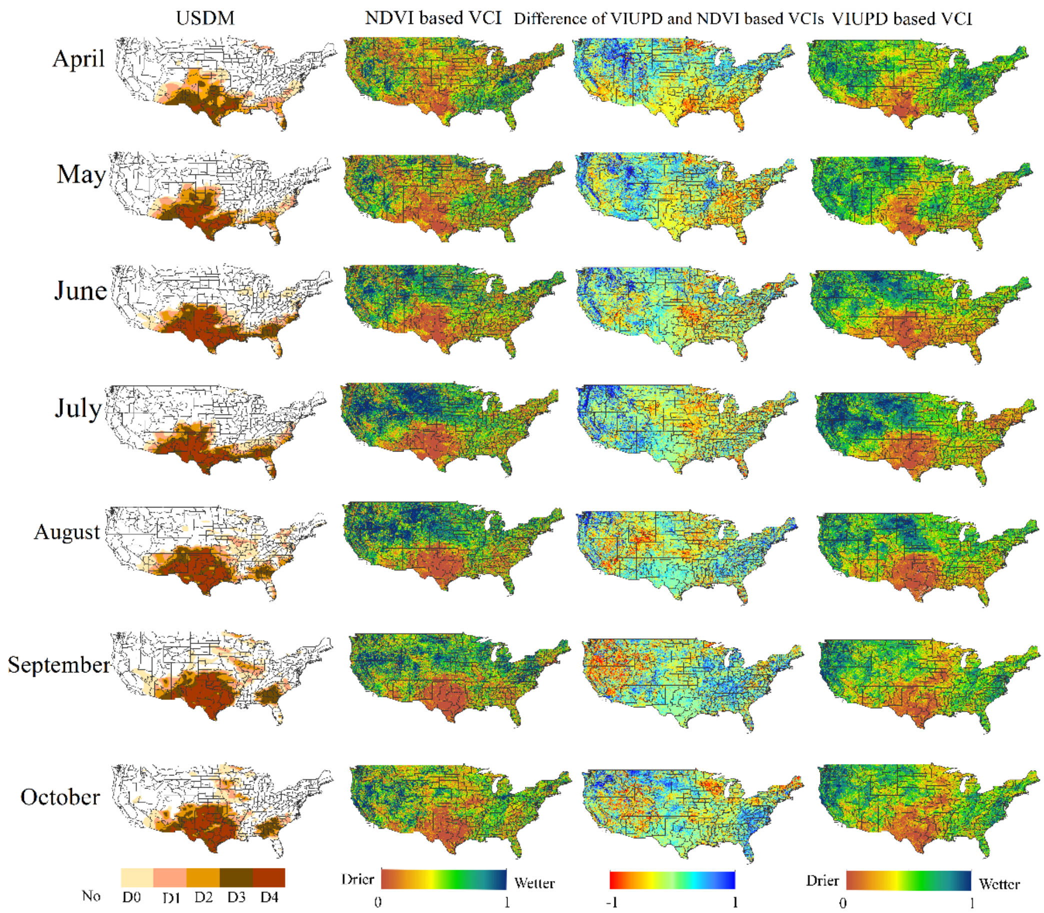

Figure 2. Drought detected by USDM, VIUPD-derived VCI and NDVI-derived VCI for April to October 2011 over the CONUS. The first column is the USDM, the second column is the NDVI-derived VCI, the third column is the VIUPD-based VCI minus the NDVI-derived VCI, and the last column is the VIUPD-derived VCI.

Based on the USDM, drought conditions were mainly located in the south, covering the majority of Texas, while New Mexico and Georgia also experienced serious drought conditions. These drought conditions became more severe by October 2011. North regions such as Michigan, Iowa and Illinois and Georgia and Alabama in southeastern regions began to suffer drought from August. For NDVI-derived VCI, severe drought appeared in The Great Plain and northeastern and northwestern regions in April and May. Then from June to August, the severe drought disappeared in north and mainly located in south regions such as Texas. In September and October, the south regions drought severity seems to reduce and north regions of The Great Plain experienced more severe drought conditions. According to VIUPD-derived VCI, the drought area mainly located in south and northeastern regions such as New York experienced severe drought in July. The south drought areas expanded and Michigan, Iowa and Illinois began to suffer drought from September to October.

The VIUPD-derived VCI described the spatial extent of the drought over the south of the CONUS reasonably well. From April to October 2011, the VIUPD-derived VCI indicated more severe drought conditions than the NDVI-derived VCI in eastern Texas, most of New Mexico, and the southeastern CONUS. These areas were confirmed to be experiencing severe drought conditions by USDM. In regions in which no drought conditions were detected, the VIUPD-derived VCI indicated less-severe drought conditions than the NDVI-derived VCI. In the west and northwest of the CONUS, from April to October 2011 normal conditions were experienced according to USDM. The map showing the difference between the VIUPD and NDVI-derived VCI (column 3) showed that in these regions the VIUPD-derived VCI had higher values than the NDVI-derived VCI. The NDVI-derived VCI indicated more severe drought conditions than the VIUPD-derived VCI in the regions classified as experiencing no drought. It is even more obvious that in April and June of 2011, NDVI-derived VCI showed significantly more regions with severe drought conditions than VIUPD-derived VCI in the north and northwestern regions of the COUNS, while these regions were not detected as drought conditions by the USDM.

Similar to the NDVI-derived VCI, the VIUPD-derived VCI may also produce false drought signals. For example, in the northwestern and northeastern regions, from New York to Maine, the VIUPD-derived VCI indicated more severe drought conditions than USDM. VIUPD-derived VCI underestimated drought level as compared to the results of USDM and NDVI-derived VCI in southern States including Alabama and Georgia in September and October. However, on the whole, the VIUPD based VCI showed more similarity to USDM than the NDVI-based VCI. The mere fact that the overall performance of VIUPD-derived VCI is better than NDVI-derived VCI is not enough to prove that VIUPD-derived VCI can reasonably monitor drought condition for a long time. The correlations with *in situ* drought indices for 10 years (2002–2011) were analyzed in the next section.

3.3. Comparison of the Spatial Variability of the VIUPD and NDVI Derived VCIs

Figure 3 shows maps describing the spatial variability and average correlation coefficients of the NDVI-derived VCI and VIUPD-derived VCI, and the corresponding values for station-based indices from April to October 2002–2011. Spatially, the NDVI-derived VCI produced stronger correlations with PDSI, SPI-3, SPI-6, and SPI-9 than with SPI-1, SPI-2, or the Z-index. The high correlation values ($r > 0.7$) were mainly located in southeastern areas, such as Texas, New Mexico, and Arizona. Due to the strong influence of environmental factors, such as mean annual precipitation, permeability, and irrigation [4], the NDVI-derived VCI had a low correlation in the northwestern and northeastern United States. As shown in Figure 2, in general, the spatial variability of VIUPD-derived VCI is similar to NDVI-derived VCI, but the VIUPD-derived VCI can significantly increase the correlation with station-based drought indices. When correlated to the station-based drought indices, the VIUPD-derived VCI produced strong correlations for more climate divisions than the NDVI-derived VCI did. While, for the VIUPD-derived VCI, the high correlation values ($r > 0.7$) were located in southern regions (e.g., Texas) and western regions (e.g., California and Nevada), and also in humid-hot regions in the southeastern CONUS (e.g., Florida). Weaker correlations were found mainly in humid areas for the NDVI-derived VCI, whereas the VIUPD-derived VCI exhibited significantly improved performance in humid areas. Similarly to the NDVI-derived VCI, the VIUPD-derived VCI produced weaker correlations with *in situ* drought indices in humid regions in the northeastern area around the Great Lakes, between the US and Canada, and in evergreen forest regions in the northwest. However, the VIUPD-derived VCI also produced stronger correlations in other humid CDs in the eastern and northwestern CONUS than NDVI-derived VCI (see Figure 3).

In addition, in order to make a comprehensive comparison between VIUPD-derived VCI and NDVI-derived VCI, when correlated to *in situ* drought indices, the number of CDs which passed at least p-value of 0.05 for testing statistical significance is measured (in Figure 4). Figure 4 indicated that both VIUPD-derived VCI and NDVI-derived VCI have fewer CDs that passed the p-value test for correlating to SPI-1, and more CDs when correlating to PDSI. It is also obvious that there are many more CDs that passed the p-value test for VIUPD-derived VCI than NDVI-derived VCI correlating to all station-based drought indices.

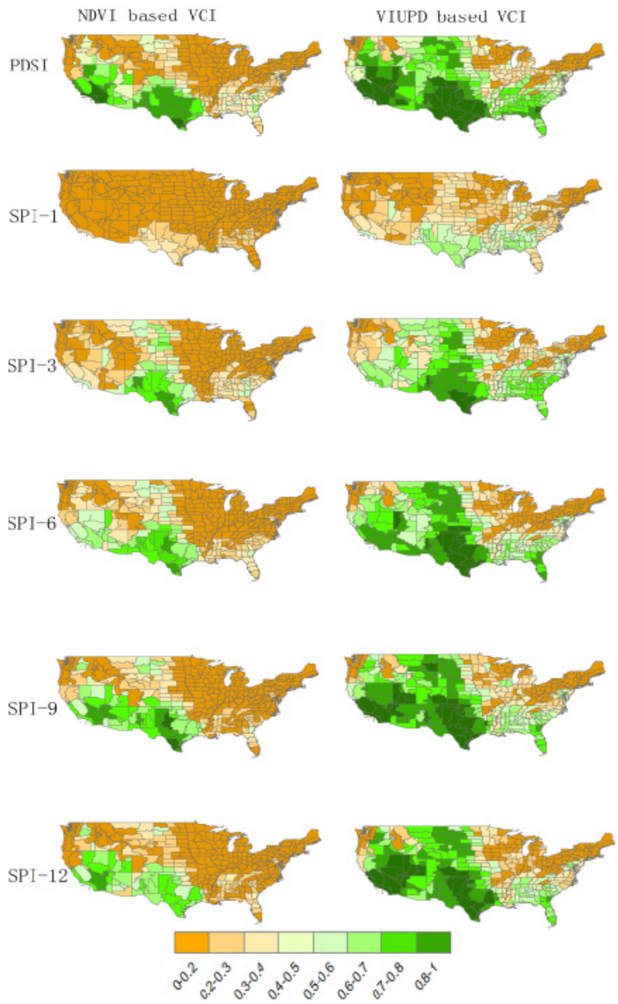

Figure 3. Spatial distribution of climate divisions with the correlations (r-value) between remote-sensing-based VCI and *in situ* drought indices for the entire growing season (April to October).

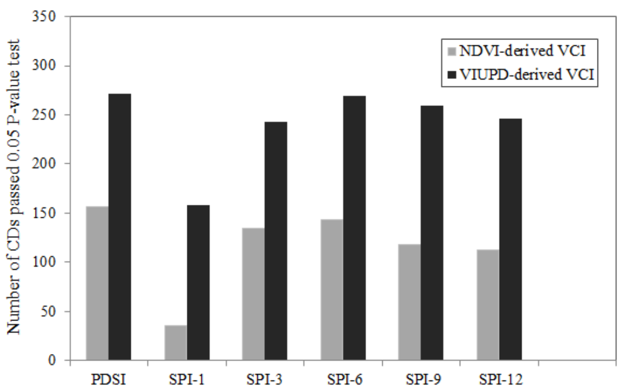

Figure 4. The number of climate divisions (CDs) passed at least *p*-value of 0.05 for testing statistical significance when comparing VI-based VCIs and station-based drought indices. *X*-axis stands for the station based drought indices which NDVI and VIUPD-derived VCIs are correlated to. *Y*-axis stands for the number of CDs which passed at least *p*-value of 0.05 for testing statistical significance.

To further evaluate the drought-monitoring ability of the VIUPD-derived VCI, the performance of the VIUPD-derived VCI and NDVI-derived VCI were compared in three sub-periods (April to May, June to July, and August to September). It can be seen from Figure 5 and Table 6 that the r-values of NDVI and VIUPD based VCIs varied among the sub-periods. Both the VIUPD-derived VCI and NDVI-derived VCI performed better in June to July and August to September than in April to May. Ji *et al.* [3] indicated that vegetation response to moisture availability varies significantly between months, and it depends on the plant growth stage. During the period that vegetation develops reproductive organs, drought has the greatest effect on vegetation health, thus the vegetation is more sensitive to drought conditions during the rapid growing months. The results of experiments conducted by Ji *et al.* [3] showed that the relationship between vegetation and 3-month SPI in June to September is stronger than in May is agreed with our studies. On the other hand, the fact that VIUPD-derived VCI exhibited significantly stronger correlations with *in situ* drought indices than the NDVI-derived VCI did in all sub-periods, cropland- and grassland-dominated climate divisions indicated that VIUPD-derived VCI are not only more sensitive to vegetation moisture demand in rapid growing season but also the beginning of the vegetation growth. The VIUPD-derived VCI and NDVI-derived VCI generally displayed a similar trend with regard to their correlations with *in situ* drought indices in all sub-periods of the growing season. At the start of the growing season (April to May), the correlation between the VIUPD-derived VCI and SPI-1 differed markedly from that of the NDVI-derived VCI. The VIUPD-derived VCI exhibited a considerably greater number of climate divisions with r-values higher than 0.4 compared to the NDVI-derived VCI, and there was also a stronger correlation with SPI-1 over the whole CONUS (Figure 5).

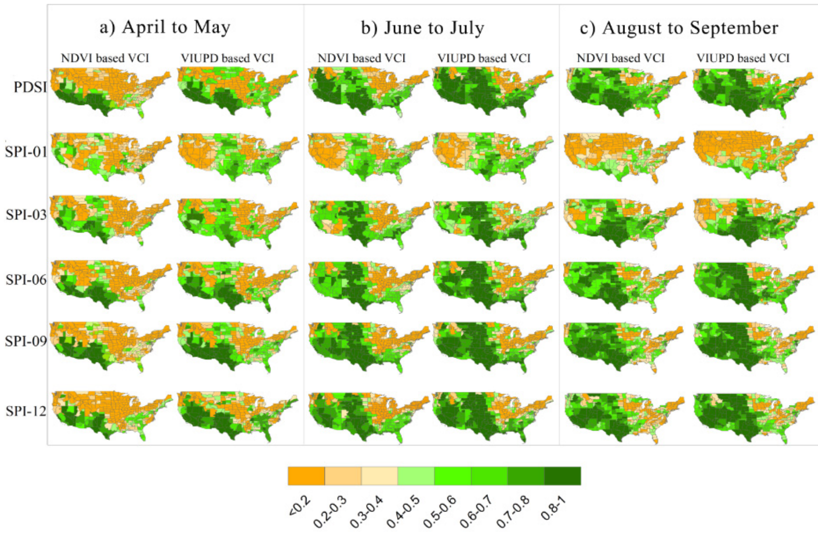

Figure 5. Spatial distribution of climate divisions with correlations (r-value) between VIUPD and NDVI-derived VCIs, and *in situ* drought indices for the three sub-periods from April to September. The sub-figure (**a**) stands for the correlations (r-value) from April to May; the sub-figure (**b**) stands for the correlations (r-value) from June to July, sub-figure (**c**) stands for the correlations (r-value) from August to September.

Table 6. Comparisons between VIUPD and NDVI-derived VCIs in different sub-periods of the growing season.

Month	Drought Indices	r (n = 6880)							
		PDSI	Z	SPI-1	SPI-3	SPI-6	SPI-9	SPI-12	SPI-24
April–May	VIUPD-VCI	0.351	0.339	0.425	0.381	0.360	0.429	0.385	0.326
	NDVI-VCI	0.257	0.269	0.293	0.329	0.315	0.265	0.191	0.117
Jun–July	VIUPD-VCI	0.750	0.699	0.463	0.531	0.601	0.651	0.643	0.550
	NDVI-VCI	0.527	0.485	0.355	0.417	0.383	0.428	0.446	0.312
August–September	VIUPD-VCI	0.768	0.529	0.402	0.647	0.699	0.723	0.684	0.514
	NDVI- VCI	0.552	0.338	0.226	0.476	0.475	0.493	0.444	0.374

3.4. Comparison of the Spatial Variability of VIUPD-Derived VCI and Other Remote-Sensing-Based Single Drought Indices

The TCI, PCI and SMCI are widely used remote-sensing-based single drought indices [2,35]. To assess the ability of VIUPD-derived VCI to monitor drought, the spatial patterns of VIUPD-derived VCI and the widely used remote-sensing-based single drought indices were compared for April to October 2002–2011 (Figure 6 and Tables 3–5).

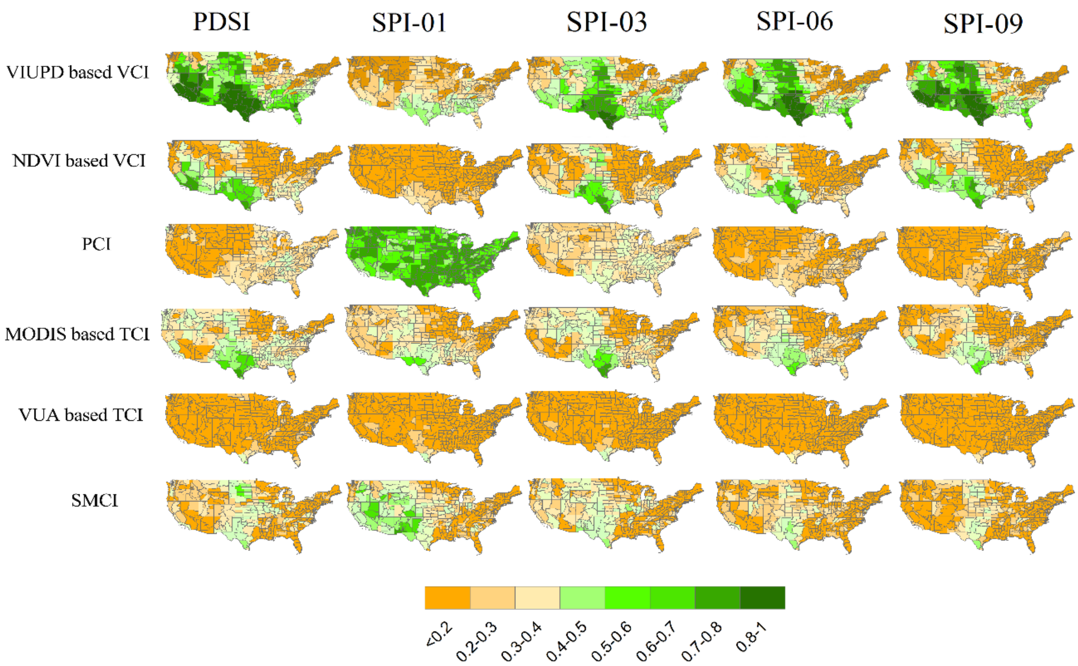

Figure 6. Spatial distribution of climate divisions with correlations (r-value) between VIUPD-derived VCI and other commonly used remote-sensing-based single drought indices with *in situ* drought indices for the entire growing season (April to October) 2002–2011.

The spatial patterns detected by the drought indices differed substantially (Figure 6). Each drought index has its own strengths and limitations. As shown in Figure 6, MODIS-derived TCI, NDVI-derived VCI and VIUPD-derived VCI presented a similar spatial variability. There were higher correlations with PDSI and long-term SPI in warm southern regions for MODIS-derived TCI, but lower correlations in northeastern regions such as Minnesota. PCI exhibited stronger correlations with SPI-1 in almost all parts of the CONUS than the other indices. Additionally, PCI showed a stronger correlation with SPI-3 than NDVI-derived VCI, MODIS-derived TCI and SMCI in the eastern and western CDs. However, the correlations of PCI and longer-term SPI indices are lower in most of the CONUS. The correlations of PCI and SPI-6 and SPI-9 are lower than those of NDVI and VIUPD-derived VCIs, MODIS-derived TCI and SMCI in the majority of CDs. SMCI showed stronger correlation with *in situ* indices than the short-term SPI indices, and showed a weak correlations with PDSI and long-term SPIs for most areas. SMCI is better-suited to monitor the short-term drought conditions of large geographical regions. When compared to other indices, SMCI is particularly sensitive to terrain. As shown in Figure 1, the northeastern areas of Minnesota and Wisconsin are covered by large forests and wetlands, and the r-values of SMCI in these regions were lower than those of cropland or herbaceous regions. The same trend was evident in the eastern areas of deciduous forest, and the northwestern areas of evergreen forests. However, the correlation of SMCI and SPI-1 is higher than that of MODIS-derived TCI in regions of low vegetation density, and with few forests.

In order to explore the different performances of VIUPD-derived VCI and other remote sensing-based drought indices in different conditions, we calculated the mean temperature and mean NDVI of each CD in the growing season from 2002 to 2011 (Figure 7). The differences of r-values between VIUPD-derived VCI and other drought indices in each CD (r-values of VIUPD-derived VCI minus r-values of other remote sensing-based drought indices in each CD, see Figure 8) were also calculated. As shown in Figure 8, when correlated to *in situ* drought indices, the VIUPD-derived VCI has higher r-values than NDVI-derived VCI in almost all different CDs. When compared to PCI, even the VIUPD-derived VCI performed much better than it did in correlating to long term drought indices such as PDSI, SPI-06 and SPI-09, the VIUPD-derived VCI has much lower correlations with short term SPI than PCI in almost all the CDs. In addition, the VIUPD-derived VCI showed higher r-values than SMCI in the southeastern regions where the mean NDVI is above 0.6 (see Figures 7 and 8). It also should be noticed that the VIUPD-derived VCI performed better than VUA based TCI in all different conditions. However, when compared to MODIS based TCI, even the VIUPD-derived VCI had higher r-values in the hot regions such as CDs of California and Arizona in the southwest regions, it performed worse in cold regions such as Washington. As shown in Figure 6, the performance of MODIS based TCI was worse in the extremely hot regions (CDs in Arizona and New Mexico) and cold regions (northeastern CDs like Michigan and New York to Maine) than other regions, the VIUPD-derived VCI can greatly improve the performance of TCI in hot regions but not in the cold regions.

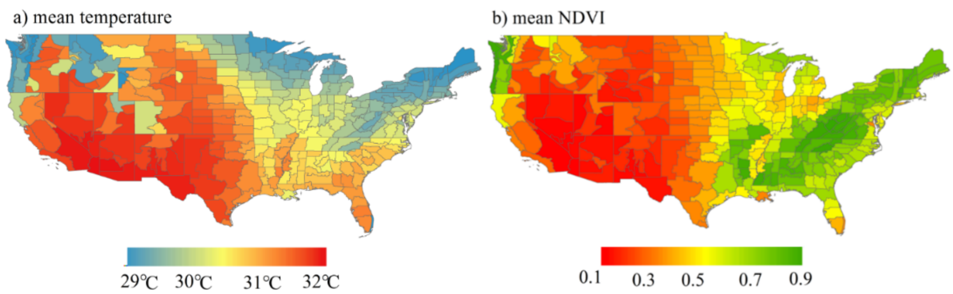

Figure 7. The mean temperature and mean NDVI of each CD in the growing season from 2002 to 2011. The sub-figure (**a**) is the mean temperature and sub-figure (**b**) is the mean NDVI of each CD in the growing season from 2002 to 2011. In the sub-figure (**a**), the red color stands for the warmer temperature and the blue color stands for the cooler temperature; in the sub-figure (**b**), red color stands for the lower NDVI and green color stands for the higher NDVI.

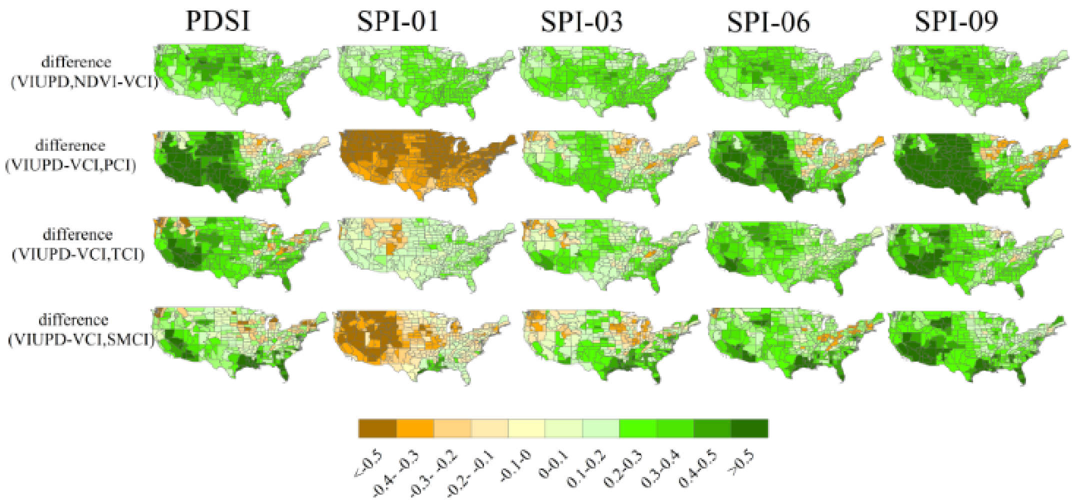

Figure 8. Spatial distribution of climate divisions with correlations (r-value) difference between VIUPD-derived VCI and other commonly used remote-sensing-based drought indices. The difference means the r-value of VIUPD-derived VCI in each CD minus the r-value of other drought indices.

Even the VIUPD-derived VCI has higher correlations with *in situ* drought indices in most of CDs of the continental United States than other drought indices compared, it should be noticed that the VIUPD-derived VCI has its own limitations and applicability. Under some circumstances, the VIUPD-derived VCI should be used with caution. As shown in Figure 9, the performance of VIUPD-derived VCI was greatly correlated to the mean temperature of the growing season. When correlated to *in situ* drought indices of PDSI, Z-index, 3-, 6-, 9- and 12-month of SPI, the r-values of VIUPD-derived VCI had a good relation with temperature. Especially for PDSI, when VIUPD-derived VCI correlated to it, the coefficient of determination (R^2) of r-value and temperature was as high as 0.7616. It indicates that when correlated to PDSI, 76.16% of the performances in the CDs were influenced by temperature. When VIUPD-derived VCI correlated to Z-index, 3-, 6-, 9-, 12-month SPI, the coefficients of determination are also high (0.6569, 0.5566, 0.6756, 0.7577 and 0.7127 for Z-index, 3-, 6-, 9-, 12-month SPI respectively). The R^2 for longer term SPIs (6-, 9-, 12-month SPI) was higher than shorter term SPIs (1- and 3-month SPI). In the CDs with low mean temperature, the performances of VIUPD-derived VCI were not considerable, especially the CDs with mean temperature lower than 30 °C. In addition, from Figures 7 and 8a, the CDs with worse performance of VIUPD-derived VCI are CDs with lower mean temperature than other regions. As mentioned above, at least in this study, the VIUPD-derived VCI may not be used in the cold regions, especially the regions with mean temperature of the growing season less than 30 °C.

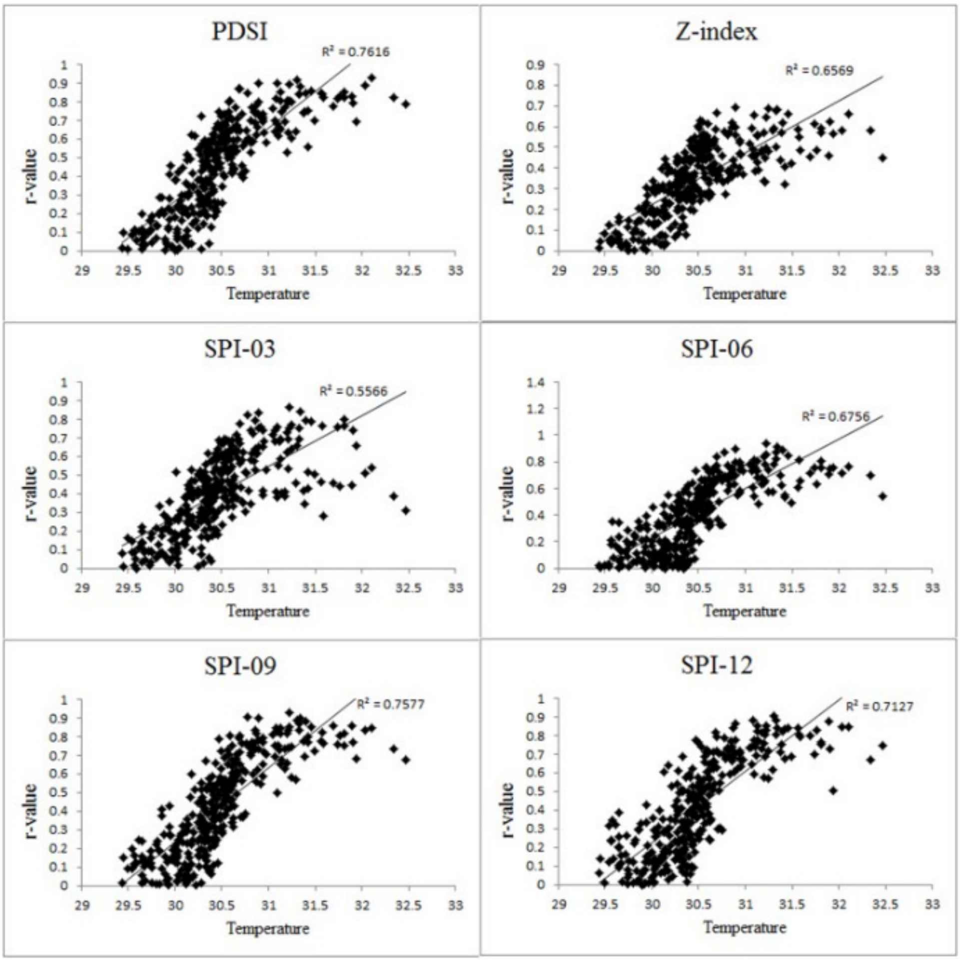

Figure 9. The correlations of r-values of VIUPD-derived VCI with *in situ* drought indices and mean temperature of the growing season from 2002 to 2011.

4. Discussion

The NDVI is widely used in various applications and it is also a commonly used index to monitor drought severity because there is a close relationship between vegetation vigor and available soil moisture, especially in arid and semiarid areas [3]. The NDVI indicates the severity of vegetation stress resulting from water stress. One of the main advantages of the NDVI-derived VCI is that, because it is a satellite-based drought product, it can provide near real-time data over the globe at a relatively high spatial resolution. In addition, the NDVI-derived VCI uses a completely independent methodology for monitoring drought, while many of the other meteorological indices rely on station-based meteorological and agricultural data. However, studies showed that, in some cases, the sensitivity of the NDVI to the water stress of vegetation is limited. The VIUPD-derived VCI is also a satellite-based drought product and can use a completely independent methodology for monitoring without station-based data being inputted.

4.1. Consistency of GPP and VIUPD

In this study, we evaluated the utility of VIUPD-derived VCI using the USDM, different time scale SPI, PDSI, Z-index, NDVI-derived VCI, VUA derived SMCI, NSIDC derived SMCI, VUA derived TCI and MODIS derived TCI. The results indicated that the VIUPD-derived VCI performed well for drought monitoring. However, the good performance of VIUPD-derived VCI must derive from the good performance of VIUPD. To evaluate the sensitivity of VIUPD to drought impact and to further validate the utility of VIUPD-derived VCI, we analyzed the consistency of GPP and VIUPD.

Figure 10 showed the inter-annual and seasonal patterns of VIUPD and GPP. In this study, we only chose the months from April to October as the study period. For the 9 sites on the whole, the VIUPD showed similar trends with GPP. According to the US National Drought Mitigation Center [36], the US-ARM site experienced a severe drought in 2006. Both of GPP and VIUPD of 2006 are much lower than that of 2005. Similar information can be found in other sites, for example, the US-Aud suffered drought ever year before 2005, accordingly the GPP and VIUPD are lower than which of 2005 and 2006.

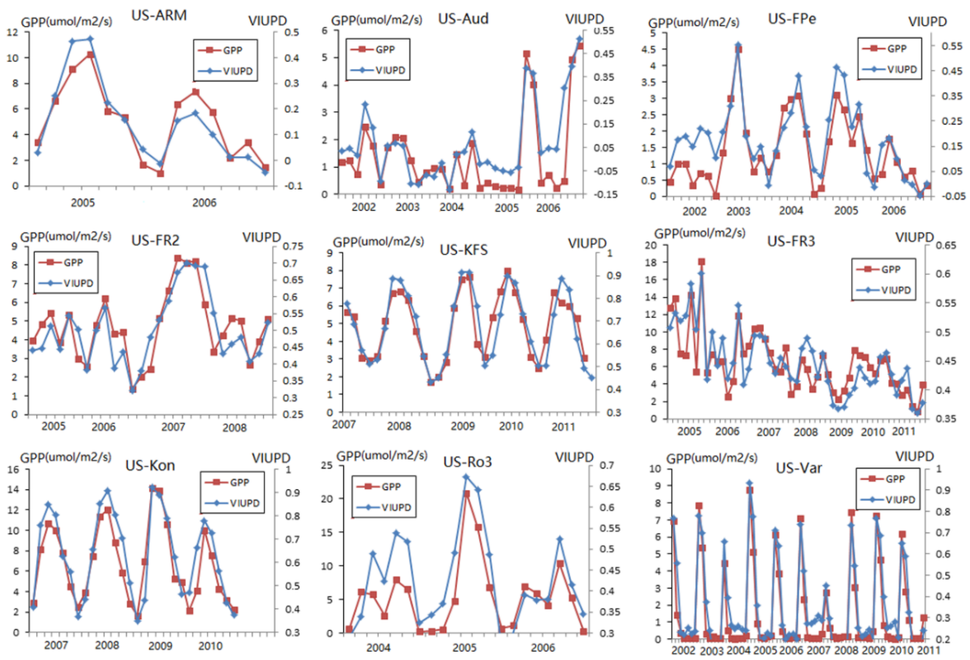

Figure 10. Seasonal patterns of VIUPD and GPP. Subfigures show the seasonal patterns of VIUPD and GPP in the flux tower sites of US-ARM, US-Aud, US-FPe, US-FR2, US-KFS, US-FR3, US-Kon, US-R03 and US-Var. The red points stand for the GPP and the blue points stand for the VIUPD.

Figure 10 shows that although the pattern of VIUPD may differ slightly from that of GPP, VIUPD remained consistent with the GPP during the growing season for both drought and non-drought years.

4.2. Facters Which Affect the Performance of VIUPD-Derived VCI

It is not surprising that the VIUPD-derived VCI is proved to be a better index than NDVI-derived VCI for measuring agricultural drought crossing the CONUS. Firstly, the NDVI uses only the red and near-infrared bands (bands 1 and 2 from MODIS data), other bands of surface reflectance, which are also sensitive to vegetation water status [37–41] can be taken into consideration to improve the sensitivity of remote sensing-based drought monitoring. In this study, we took the blue reflectance band as an example to show that the bands other than NIR and red reflectance can also have high correlations with *in situ* drought indices (see Figure 11). According to the Figure 11, the performances of the blue band and red band had similar spatial distributions, and this spatial distribution is also similar to that of NDVI and VIUPD based VCIs. In some special regions, the blue band had even higher correlations than which of NIR and red. For example, even the blue and red band had similar spatial distributions when correlated to SPI-09, the blue reflectance band had higher r-value than NIR and red reflectance band did in many CDs in the Great Plains. In the process of photosynthesis, the red and blue band are both the absorption spectra for vegetation, but previous studies suggested that blue band can reduce the effect of noise such as cloud or aerosols [42,43]. The VIUPD establishing method, which is based on the universal pattern decomposition method (UPDM), can combine and make full use of information from all the observation bands [22]. The characteristics of different bands can be combined in VIUPD. However, all the bands used cannot perform well in the cold regions, so the VIUPD-derived VCI performed worse in these regions than others did.

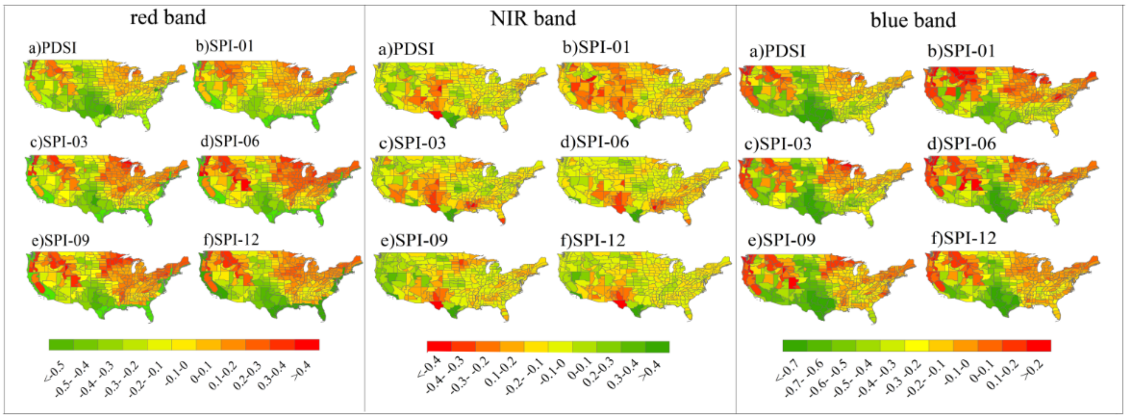

Figure 11. Spatial distribution of climate divisions with correlations (r-value) between red band, NIR band and blue band with *in situ* drought indices for the entire growing season (April to October) 2002–2011. The green color stands for the negative correlation and the red color stands for the positive correlation.

Secondly, NDVI is significantly affected by difference in spectral bandwidth, especially for the red band, and that changes in spatial resolution lead to less pervasive but more land cover specific effects on NDVI [44]. In this case, NDVI from the bandwidth of specific satellite sensor (MODIS, in this study) may not best reflect the vegetation water status in some particular regions. VIUPD has been proved to be a sensor-independent index which can greatly avoid the effect of difference in spectral bandwidth [22,23].

Thirdly, NDVI may be a limited index for monitoring the leaf status that is related to drought condition in some circumstances. The experiment in Zhang *et al.* [22] showed that the reflectance corresponding to the red and NIR bands is almost identical to that of typical yellow leaves, while for typical dead leaves, the reflectance in the red band is lower than in the infrared band.

Therefore, the NDVI of yellow leaves may be lower than that of dead leaves in some circumstances. This characteristic of the NDVI may lead to confusion for drought monitoring, because when the NDVI of dead leaves is higher than that of yellow leaves, it indicates the area of yellow leaves has experienced a worse drought condition than the area of dead leaves, which is not logical. However, the VIUPD can largely avoid this drawback of NDVI through a combination of four pattern decomposition coefficients: the patterns of vegetation, soil, water, and the supplementary pattern and yellow leaf was used as the supplementary pattern [22,36].

Some factors can also lead to the fact that VIUPD-derived VCI performed better than other commonly used remote sensing-based drought indices such as TCI, PCI and SMCI. The VIUDP-derived VCI showed better performance in many CDs than TCI. One reason is that the TCI is mainly based on the LST data and the LST data is only derived from the thermal band information. Other information except the temperature can also be a good indicator to drought. In addition, drought indices—such as PCI, and SMCI—cannot be directly obtained from the surface reflectance data, but are obtained from inversion models from the observation sensors. The inversion algorithm itself is a key factor that affects the drought-monitoring performance of the indices. For example, there was a large difference between the VUA-based TCI and MODIS-based TCI [2,35]. SMCI did not function better in areas with a high density of vegetation cover and high temperature than VIUPD-derived VCI. That is because SMCI is based on the microwave data, and the microwave brightness temperatures at X and C band are sensitive to only the soil moisture in the top 1 to 1.5 cm of the soil, when the vegetation density is too great, the revision model will not achieve convergence [45].

This study analyzed the utility of VIUPD-derived VCI for drought monitoring; overall, VIUPD-derived VCI showed better performance than NDVI-derived VCI and other commonly used drought indices. However, the VIUPD-derived VCI still has its own limitations and applicability. Analysis shown above indicated that the performance of VIUPD-derived VCI was greatly correlated to temperature. When in the CDs with lower temperature, the VIUPD-derived VCI performed worse. This may because the bands which used to establish VIUPD were the seven bands from the MOD09A1 product. These bands used had a worse performance for drought monitoring in the colder regions. Future studies would evaluate the sensitivity of VIUPD-derived VCI based on other, different bands. Siheng Wang *et al.* [46] monitored the drought condition using SIF data, future study can also include SIF information for establishing VIUPD. There are still some uncertainties affecting the analysis of this study. First of all, we have to admit that there is no absolute "true" drought measure. By using USDM, SPI, PDSI and Z-index as the standard for comparison, they establish a base level and the fact that the USDM, SPI, PDSI and Z-index have a certain level of subjectivity because of individuals' reports. There is still a possibility that these indices which used as standard did not properly monitor the drought condition. Other factors may also affect the results of this research, such as the remaining cloud noise of the images and spatial resolution.

This study also presented a new way to calculate VCI. Almost all the studies used VCI based on NDVI. Our research indicated that the establishment of VCI should not be limited in NDVI, and VIUPD can also be a good vegetation index to build VCI. Other future applications can also build VCI based on other superior vegetation index under specific circumstances. This study only focused on the utility of VIUPD-derived VCI for drought monitoring and compared VIUPD-derived VCI with other commonly used remote sensing based drought indices. Future work should focus on why the VIUPD-derived VCI is limited in its performance for short-term drought monitoring and what factors could affect the performance of VIUPD-derived VCI.

5. Conclusions

This study assessed the spatial and temporal performances of the VIUPD-derived VCI in comparison with the NDVI-derived VCI, TCI, SMCI, PCI in various climate divisions across the CONUS. The remote-sensing-based drought indices (VIUPD-derived VCI, NDVI-derived VCI, VUA based TCI, MODIS based TCI, TRMM based PCI, and AMSR-E based SMCI) were correlated with the *in situ* drought indices (PDSI, Z-index, SPI-1, SPI-3, SPI-6, SPI-9, SPI-12, and SPI-24).

The VIUPD-derived VCI had the strongest correlation with *in situ* drought indices in different sub-periods of the growing season and in a greater number of climate divisions, with higher r-values than the NDVI-derived VCI. This indicates that the VIUPD has the potential for monitoring drought conditions in different environments. Compared with the other single remote-sensing-based drought indices (TCI, PCI, and SMCI), the VIUPD-derived VCI was more suitable for longer-term drought monitoring, such as agricultural droughts, because it had stronger correlations with SPI-6, SPI-9, SPI-12, SPI-24, and PDSI. The VIUPD-derived VCI can also overcome some of the defects of SMCI for short-term drought monitoring in areas with a high density of vegetation cover. As VIUPD can make use of the information from all the observation bands, the VIUPD-derived VCI can be regarded as an enhanced VCI. The VIUPD-derived VCI is recommended as the optimum remote-sensing-based single drought index for long-term drought in the warm regions over the CONUS.

Acknowledgments: This work was supported under the Natural Science Foundation of China (Project Numbers 41371362, 41201348, and 41202234) opening fund of the National Key Laboratory of Remote Sensing Science (OFSLRSS201508).

Author Contributions: Lifu Zhang, Qingxi Tong and Wenzhe Jiao conceived and designed the study; Wenzhe Jiao and Qing Chang carried out the investigation; Dongjie Fu and Yi Chen reviewed the manuscript; Wenzhe Jiao wrote the manuscript. All co-author provided supervision of the manuscript throughout the process.

Conflicts of Interest: The authors declare no conflict of interests.

Abbreviations

The following abbreviations are used in this manuscript:

NDVI	Normalized Difference Vegetation Index
VIUPD	Vegetation Index based on the Universal Pattern Decomposition Method
VCI	Vegetation Condition Index
TCI	Temperature Condition Index
PCI	Precipitation Condition Index
SMCI	Soil Moisture Condition Index
CONUS	Continental United States
PDSI	Palmer Drought Severity Index
SPI	Standardized Precipitation Index
EVI	Enhanced Vegetation Index
MCARI	Modified transformed Chlorophyll Absorption Ratio Index
TVI	Triangle Vegetation Index
TRMM	Tropical Rainfall Measuring Mission
NASA	National Aeronautics and Space Administration
MODIS	Moderate-resolution Imaging Spectroradiometer
GPP	Gross Primary Production
CD	Climate Division
UPDM	Universal Pattern Decomposition Method

References

1. Heim, R.R., Jr. A review of twentieth-century drought indices used in the United States. *Bull. Am. Meteorol. Soc.* **2002**, *83*, 1149–1165.
2. Zhang, A.; Jia, G. Monitoring meteorological drought in semiarid regions using multi-sensor microwave remote sensing data. *Remote Sens. Environ.* **2013**, *134*, 12–23. [CrossRef]
3. Ji, L.; Peters, A.J. Assessing vegetation response to drought in the northern Great Plains using vegetation and drought indices. *Remote Sens. Environ.* **2003**, *87*, 85–98. [CrossRef]

4. Palmer, W.C. *Meteorological Drought*; US Department of Commerce, Weather Bureau: Washington, DC, USA, 1965.
5. McKee, T.B.; Doesken, N.J.; Kleist, J. The relationship of drought frequency and duration to time scales. In Proceedings of the 8th Conference on Applied Climatology, Anaheim, CA, USA, 17–22 January 1993; American Meteorological Society: Boston, MA, USA; pp. 179–183.
6. Rhee, J.; Im, J.; Carbone, G.J. Monitoring agricultural drought for arid and humid regions using multi-sensor remote sensing data. *Remote Sens. Environ.* **2010**, *114*, 2875–2887. [CrossRef]
7. Wu, J.; Zhou, L.; Liu, M.; Zhang, J.; Leng, S.; Diao, C. Establishing and assessing the Integrated Surface Drought Index (ISDI) for agricultural drought monitoring in mid-eastern China. *Int. J. Appl. Earth Obs. Geoinf.* **2013**, *23*, 397–410. [CrossRef]
8. Kogan, F.N. Droughts of the late 1980s in the United States as derived from NOAA polar-orbiting satellite data. *Bull. Am. Meteorol. Soc.* **1995**, *76*, 655–668. [CrossRef]
9. Domenikiotis, C.; Spiliotopoulos, M.; Tsiros, E.; Dalezios, N. Early cotton yield assessment by the use of the NOAA/AVHRR derived Vegetation Condition Index (VCI) in Greece. *Int. J. Remote Sens.* **2004**, *25*, 2807–2819. [CrossRef]
10. Kuri, F.; Murwira, A.; Murwira, K.S.; Masocha, M. Predicting maize yield in Zimbabwe using dry dekads derived from remotely sensed Vegetation Condition Index. *Int. J. Appl. Earth Obs. Geoinf.* **2014**, *33*, 39–46. [CrossRef]
11. Liu, W.; Kogan, F. Monitoring Brazilian soybean production using NOAA/AVHRR based vegetation condition indices. *Int. J. Remote Sens.* **2002**, *23*, 1161–1179. [CrossRef]
12. Seiler, R.; Kogan, F.; Sullivan, J. AVHRR-based vegetation and temperature condition indices for drought detection in Argentina. *Adv. Space Res.* **1998**, *21*, 481–484. [CrossRef]
13. Shen, Y.; Liu, X.; Huang, Y. Impacts of crop rotation on vegetation condition index for species-level drought monitoring. In Proceedings of the Third International Conference on Agro-Geoinformatics (Agro-Geoinformatics 2014), Beijing, China, 11–14 August 2014; pp. 1–5.
14. Singh, R.P.; Roy, S.; Kogan, F. Vegetation and temperature condition indices from NOAA AVHRR data for drought monitoring over India. *Int. J. Remote Sens.* **2003**, *24*, 4393–4402. [CrossRef]
15. Wan, Z. NDVI anomaly patterns over Africa during the 1997/98 ENSO warm event. *Int. J. Remote Sens.* **2001**, *22*. [CrossRef]
16. Quiring, S.M.; Papakryiakou, T.N. An evaluation of agricultural drought indices for the Canadian prairies. *Agric. For. Meteorol.* **2003**, *118*, 49–62. [CrossRef]
17. Kogan, F.N. Global drought watch from space. *Bull. Am. Meteorol. Soc.* **1997**, *78*, 621–636. [CrossRef]
18. Gitelson, A.A.; Kogan, F.; Zakarin, E.; Spivak, L.; Lebed, L. Using AVHRR data for quantitive estimation of vegetation conditions: Calibration and validation. *Adv. Space Res.* **1998**, *22*, 673–676. [CrossRef]
19. Bayarjargal, Y.; Karnieli, A.; Bayasgalan, M.; Khudulmur, S.; Gandush, C.; Tucker, C. A comparative study of NOAA-AVHRR derived drought indices using change vector analysis. *Remote Sens. Environ.* **2006**, *105*, 9–22. [CrossRef]
20. Quiring, S.M.; Ganesh, S. Evaluating the utility of the Vegetation Condition Index (VCI) for monitoring meteorological drought in Texas. *Agric. For. Meteorol.* **2010**, *150*, 330–339. [CrossRef]
21. Dogan, S.; Berktay, A.; Singh, V.P. Comparison of multi-monthly rainfall-based drought severity indices, with application to semi-arid Konya closed basin, Turkey. *J. Hydrol.* **2012**, *470*, 255–268. [CrossRef]
22. Zhang, L.; Furumi, S.; Muramatsu, K.; Fujiwara, N.; Daigo, M.; Zhang, L. A new vegetation index based on the universal pattern decomposition method. *Int. J. Remote Sens.* **2007**, *28*, 107–124. [CrossRef]
23. Chen, X.; Zhang, L.; Zhang, X.; Liu, B. Comparison of the sensor dependence of vegetation indices based on Hyperion and CHRIS hyperspectral data. *Int. J. Remote Sens.* **2013**, *34*, 2200–2215. [CrossRef]
24. Liu, K.; Su, H.; Zhang, L.; Yang, H.; Zhang, R.; Li, X. Analysis of the urban heat island effect in Shijiazhuang, China using satellite and airborne data. *Remote Sens.* **2015**, *7*, 4804–4833. [CrossRef]
25. Jiang, H.-L.; Yang, H.; Chen, X.P.; Wang, S.D.; Li, X.K.; Liu, K.; Cen, Y. Research on accuracy and stability of inversing vegetation chlorophyll content by spectral index method. *Spectrosc. Spectr. Anal.* **2015**, *35*, 975–981.
26. National Climatic Data Center. Available online: http://www.ncdc.noaa.gov (accessed on 8 March 2016).
27. Brown, J.F.; Wardlow, B.D.; Tadesse, T.; Hayes, M.J.; Reed, B.C. The Vegetation Drought Response Index (VegDRI): A new integrated approach for monitoring drought stress in vegetation. *GISci. Remote Sens.* **2008**, *45*, 16–46. [CrossRef]

28. Du, L.; Tian, Q.; Yu, T.; Meng, Q.; Jancso, T.; Udvardy, P.; Huang, Y. A comprehensive drought monitoring method integrating MODIS and TRMM data. *Int. J. Appl. Earth Obs. Geoinf.* **2013**, *23*, 245–253. [CrossRef]
29. Guttman, N.B. Accepting the standardized precipitation index: A calculation algorithm. *J. Am. Water Resour. Assoc.* **1999**, *35*, 311–322. [CrossRef]
30. AmeriFlux. Available online: http://ameriflux.lbx.gov/ (accessed on 8 March 2016).
31. Land Processes Distributed Active Center (LPDAAC). Available online: http://lpdaac.usgs.gov/ (accessed on 8 March 2016).
32. National Aeronautics and Space Administration's (NASA) Earth Observing System Data and Information system (EOSDIS). Available online: http://reverb.echo.nasa.gov (accessed on 8 March 2016).
33. Vrije Universtiteit Amsterdam. Available online: http://nsidc.org/ (accessed on 8 March).
34. United States drought monitor (USDM). Available online: http://drought.unl/dm/ (accessed on 8 March 2016).
35. Hao, C.; Zhang, J.; Yao, F. Combination of multi-sensor remote sensing data for drought monitoring over Southwest China. *Int. J. Appl. Earth Obs. Geoinf.* **2015**, *35 Pt B*, 270–283. [CrossRef]
36. US National Drought Mitigation Center. Available online: http://drought.unl.edu (accessed on 8 March 2016).
37. Zhang, L.; Fujiwara, N.; Furumi, S.; Muramatsu, K.; Daigo, M.; Zhang, L. Assessment of the universal pattern decomposition method using MODIS and ETM+ data. *Int. J. Remote Sens.* **2007**, *28*, 125–142. [CrossRef]
38. Ceccato, P.; Flasse, S.; Tarantola, S.; Jacquemoud, S.; Grégoire, J.-M. Detecting vegetation leaf water content using reflectance in the optical domain. *Remote Sens. Environ.* **2001**, *77*, 22–33. [CrossRef]
39. Chen, D.; Huang, J.; Jackson, T.J. Vegetation water content estimation for corn and soybeans using spectral indices derived from MODIS near-and short-wave infrared bands. *Remote Sens. Environ.* **2005**, *98*, 225–236. [CrossRef]
40. Fensholt, R.; Sandholt, I. Derivation of a shortwave infrared water stress index from MODIS near-and shortwave infrared data in a semiarid environment. *Remote Sens. Environ.* **2003**, *87*, 111–121. [CrossRef]
41. Wang, L.; Qu, J.J.; Hao, X.; Zhu, Q. Sensitivity studies of the moisture effects on MODIS SWIR reflectance and vegetation water indices. *Int. J. Remote Sens.* **2008**, *29*, 7065–7075. [CrossRef]
42. Jiang, Z.; Huete, A.R.; Didan, K.; Miura, T. Development of a two-band enhanced vegetation index without a blue band. *Remote Sens. Environ.* **2008**, *112*, 3833–3845. [CrossRef]
43. Kaufman, Y.J.; Wald, A.E.; Remer, L.A.; Gao, B.-C.; Li, R.-R.; Flynn, L. The MODIS 2.1-µm channel-correlation with visible reflectance for use in remote sensing of aerosol. *IEEE Trans. Geosci. Remote Sens.* **1997**, *35*, 1286–1298. [CrossRef]
44. Teillet, P.M.; Staenz, K.; William, D.J. Effects of spectral, spatial, and radiometric characteristics on remote sensing vegetation indices of forested regions. *Remote Sens. Environ.* **1997**, *61*, 139–149. [CrossRef]
45. Owe, M.; De Jeu, R.A.M.; Holmes, T.R.H. Multisensor historical climatology of satellite-derived global land surface moisture. *J. Geophys. Res.* **2008**, *113*, F01002. [CrossRef]
46. Wang, S.; Huang, C.; Zhang, L.; Lin, Y.; Cen, Y.; Wu, T. Monitoring and assessing the 2012 drought in the great plains: Analyzing satellite-retrieved solar-induced chlorophyll fluorescence, drought indices, and gross primary production. *Remote Sens.* **2016**, *8*. [CrossRef]